nature cities

Article

https://doi.org/10.1038/s44284-026-00532-x

Nested economies of scale in global city mass

Received: 29 August 2025

Accepted: 14 September 2026

Published online: 26 October 2026

Check for updates

Kangning Huang [1,2,4] & Mingzhen Lu [3,4]

A long-standing puzzle in urban science is whether there is an intrinsic match between human populations and the mass of their built environments. Existing models assume proportionality: each additional resident demands the same amount of building material. Our analysis of more than 3,000 cities worldwide challenges this linear assumption. Built mass grows more slowly than population (that is, sublinear scaling), across cities ($\beta = 0.90$) and across neighborhoods within a city ($\delta = 0.75$). This means that larger cities and denser neighborhoods achieve economies of scale with less per capita built mass. Our theoretical framework further shows that the across-city scaling pattern emerges from the uneven within-city distribution of people. These findings caution against well-meaning interventions, such as height and building-size limits, that artificially flatten cities' natural density gradients. Effective urban policy should instead move beyond per capita linear thinking, adopting scale-adjusted metrics and managing cities as nested complex systems.

A key feature of human life is the extensive transformation of Earth's materials into built structures, establishing the biophysical foundation of modern civilization[1,2]. This capacity has intensified since the Stone Age, evolving from simple makeshift shelters in early human settlement into today's complex city built environment, where individuals find comfort and protection within individual buildings, enjoy local conveniences such as grocery shopping and schooling within vibrant neighborhoods and traverse city-wide transportation networks for professional collaborations and cultural exchanges[3].

Earth-scale data from recent breakthrough studies[1,2] have allowed us to quantify this global intensification of human material use. In particular, global per capita built mass has grown exponentially, with an approximate annual growth rate of 1.8% over the past 120+ years (Fig. 1a and Methods). Expressed dimensionlessly relative to average human body mass (~50 kg; Methods), each person now corresponds to about 4,090× their body mass in built structure (205 tonnes) (Fig. 1a). This material stock is projected to continue increasing with rising living standards worldwide[4].

Alongside the growing per capita material stock, the United Nations projects a global urban expansion of over 2 billion more residents by the mid-century[5]. Combined, this dual growth is projected to drive annual material use for urban construction and maintenance from 40 billion tonnes in 2010 to about 90 billion tonnes by 2050[6].

However, this projection has two key limitations: (1) it relies on linear models, implicitly assuming that per capita material consumption depends solely on living standards and affluence[4], independent of city size (for example, doubling population will double consumption). But recent advances[7,8] in urban scaling research challenge this assumption, showing that many urban properties scale nonlinearly with city size (for example, doubling population more than doubles economic output), making per capita predictions questionable. (2) It lacks spatial detail, overlooking substantial variations in infrastructure within cities[9,10]. This limits insight into whether nonlinear scaling holds across spatial scales, from cities to neighborhoods. These gaps—linear assumptions and low spatial resolution—hinder accurate predictions of material use and infrastructure needs across diverse urban areas, risking misguided sustainability and climate policies.

Here we map the global mass distribution of the human built stock (buildings, roads, other infrastructures). We integrate high-resolution mappings of buildings[11–13], mobility infrastructure including subway networks[14] and pavement[15] in >3,000 cities[16] with region- and type-specific material intensities[17,18] (Extended Data Figs. 1–4, Supplementary Notes 1 and 2 and Supplementary Tables 1–4).

Our analysis offers an in-depth look of the built structure vs human match in urban settings. The total built mass of cities worldwide is a staggering 327 gigatonnes, equivalent to the entire global

[1]Shanghai Key Laboratory of Urban Design and Urban Science, NYU Shanghai, Shanghai, China. [2]Division of Arts and Sciences, NYU Shanghai, Shanghai, China. [3]Department of Environmental Studies, New York University, New York, NY, USA. [4]These authors contributed equally: Kangning Huang, Mingzhen Lu. e-mail: kangning.huang@nyu.edu; mingzhen.lu@nyu.edu

https://doi.org/10.1038/s44284-026-00532-x

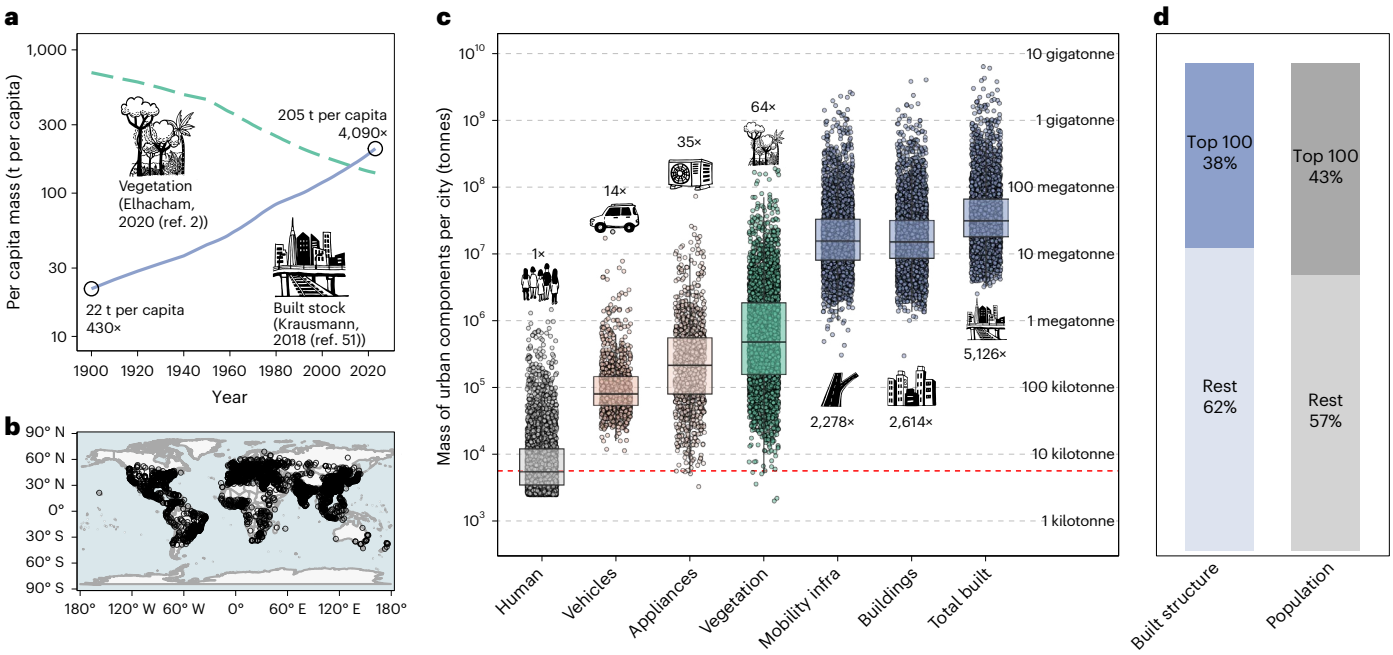


Fig. 1 | Global mass distribution of the built stock in relation to vegetation and humans. a, Per capita built stock increased exponentially from 22 t per capita in 1900 to 205 t per capita today, representing 1.8% annual growth. In contrast, per capita vegetation biomass declined from 694 t per capita to 138 t per capita, a 1.3% annual decrease. Per capita built stock is based on the global material-stock accounts of Krausmann et al.[1,51]; vegetation biomass on Elhacham et al.[2]. Historical population from Our World in Data. Values after 2015 reflect the extrapolation of Elhacham et al.[2]. Note that the *y* axis is logarithmic scale. **b**, Map of 3,593 cities included in our analysis with a size cut-off of 50,000 residents (Methods). **c**, City-level mass of the built environment is ranked according to the median value: human (gray, this study, $n = 3,757$), mobile stocks such as vehicles and appliances (light orange, Sun et al.[19], $n = 1,118$), vegetation biomass (green, Spawn et al.[52], $n = 3,752$), mobility infrastructure (labeled 'Mobility infra'; blue, this study, $n = 3,754$), buildings (blue, this study, $n = 3,757$), total built stock (blue, this study, $n = 3,754$). The red dashed line (median city-level human mass) serves as a reference threshold across categories. Scale indicators below each category (for example, 64×) denote the average multiplicative difference relative to human mass (average human body mass estimated to be 50 kg), highlighting the magnitude of resources required to support human living. **d**, The world's biggest 100 cities account for 38% of all mass and 43% of urban population. In each box plot, the lower and upper bounds of the whiskers denote minima and maxima, the center line denotes the median and the lower and upper bounds of the boxes represent the 25% and 75% quantiles, respectively. Credit: icons in **a** and **c**, Aiyu Zheng.

urban impervious area[15] (~ 0.3 M km^2) submerged under a half-meter-deep layer of solid concrete (height of a coffee table). All cities taken together, each person is supported by built stock that is >5,000 times their own mass while only enjoying vegetation 64 times their own mass (Fig. 1c). Moreover, based on a smaller regional dataset[19], we reveal mobile stock (such as vehicles, home appliances) is much heavier than human mass but dwarfed in magnitude by the built stock (<1%). As a result, the use of city mass in this paper refers to, by approximation, the mass of mass-dominant built infrastructure.

Looking beyond per capita averages, the distribution of city mass is highly right skewed (Fig. 1d): the world's heaviest 100 cities (under 3% of all cities) account for ~38% of all urban mass, equivalent to the mass of the smallest 3,331 cities combined (~90% of cities). The distribution of population is similarly more concentrated in big cities: the top 100 populous cities alone host 43% of the global urban population. Curiously, the top 100 most populous cities host a larger share of the population with disproportionately less built mass, resulting in an approximately 31% lower per capita built mass compared to the rest of the world (175 vs 253 t per capita).

This notable difference suggests that the per capita ratio may not be scale invariant and could potentially decline as cities grow larger. In the next section, we analyze the nonlinear dependence of built mass as a function of city size.

Universal across-city economies of scale

We found a consistent sublinear scaling relationship between urban built mass (M) and city size measured by population (N) across major countries of the world (Fig. 2a; $M = M_0N^{\beta}$), pointing to economies of scale in material use as cities get bigger. Most countries have a scaling slope (β) around 0.88 (<1, sublinear; standard deviation = 0.088) despite the wide range of economic development level, technology, culture of building style, climatic conditions and abundance of natural resources included in our global datasets. The distribution of scaling slopes (Fig. 2a, left inset) suggests that there's an intrinsic central tendency of the urban system around 0.88, and country-scale variations generate deviations from this central tendency in a Gaussian manner.

Note that this scaling slope (0.88) is less sublinear than the slope for road area derived from urban scaling theory (0.83) (ref. 7), which did not account for the varying per area material mass. This difference arises because the most heavily used roads require disproportionately more material per unit area (for example, thicker pavement layers)[17] to withstand higher traffic loads and ensure structural durability. As a result, built mass grows less efficiently with population than road surface area alone.

In contrast to the Gaussian distribution of slope, the intercept of the scaling relationship (M_0) has a right-skewed distribution: some countries have extremely large values while the majority of countries are much less materially developed and have small values. Intuitively, M_0 can be interpreted as the material stock required for a one-person city, reflecting the baseline material demand to support a typical city dweller. The country-scale variation in intercept follows a log-normal distribution (Fig. 2a, right inset; mean = 866 t per capita$^{\beta}$). This implies large disparities in baseline built mass across countries, shaped by factors such as income levels, construction practices and historical development.

https://doi.org/10.1038/s44284-026-00532-x

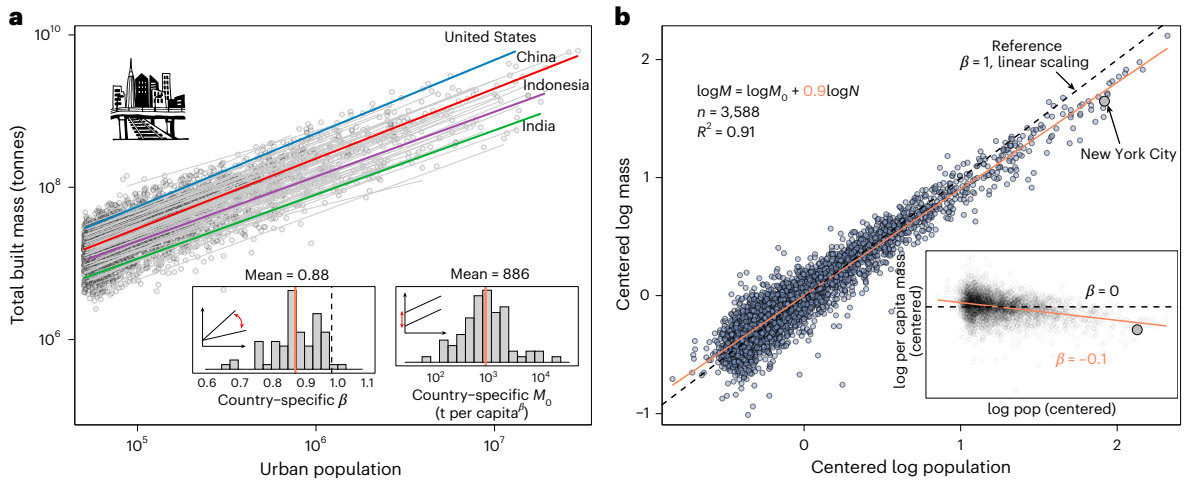


Fig. 2 | Sublinear urban scaling of built mass and variations are universal. **a**, Scatter plot of total city mass (tonnes) scales sublinearly with population across cities (gray dot) from 75 countries, indicating economies of scale in urban infrastructure materials. A country is included if they have at least five cities. We colored four example countries to highlight their similarity of slopes and variations of intercept. All other countries are denoted by gray lines (Extended Data Fig. 5 shows regressions of all countries and Extended Data Fig. 6 shows distribution of goodness of fit). The inset on the left describes the distribution of country-specific scaling slope (n = 75, mean = 0.88, median=0.88), whereas the inset on the right describes the distribution of country-specific intercept M_0 (n = 75, mean = 886 t per capita$^{\beta}$, median = 850 t per capita$^{\beta}$). **b**, After normalizing cities based on their country-specific intercepts (Methods, de-centering), the solid orange line shows the best-fit power-law scaling relationship (exponent $\beta = 0.9$, $R^2 = 0.91$, n = 3,588). The dashed black line represents the linear expectation if city mass were directly proportional to population size based on per capita average ($\beta = 1$). The inset highlights the divergence between these two lines expressed as per capita built mass, underscoring the inadequacy of linear estimates (log population labeled as 'log pop'). By definition of per capita metric, $\beta = 0.9 - 1 = -0.1$. Each blue dot represents a unique city based on our definition (Extended Data Fig. 1); we highlighted New York City as an example. Credit, icon in **a**, Aiyu Zheng.

Given the centralized distribution of scaling slope, we applied a centered-scaling approach developed by Bettencourt and Lobo[20] to remove country-specific baseline differences and characterize the general relationship between built mass and city size (Methods). We found a universal sublinear scaling relationship across all cities in our dataset (Fig. 2b; $\beta = 0.9$, 95% confidence interval = (0.89,0.91), $r^2 = 0.91$, n = 3,588, $P < 0.001$). A city with twice the population of another city only needs 87% more mass.

These sublinearity results are fairly robust to the choices of source datasets. Using each of the three independent buildings source dataset or various mixtures of these datasets (Methods) yields β from 0.892 to 0.916 (Supplementary Table 5). Moreover, the results are also insensitive to the granularity of the material intensity look-up table (Supplementary Note 2). Applying a homogeneous global average versus a 32-region detailed table shifts the scaling slope by at most 0.004 (Supplementary Table 6). Last but not least, while our built mass dataset does include subway system mass, we acknowledge that our accounting inevitably did not capture underground pipes, cables and other infrastructure that evades remote sensing (Supplementary Note 3). However, previous analysis has pointed out that metal stocks in electricity infrastructure of the new world industrial countries amounts to ~0.45 t per capita (<0.1% of the mapped built structures of the USA, 391 t per capita) (refs. 9,21). We expect future efforts that explicitly map subsurface infrastructure will further refine these estimates.

As a consequence of this sublinear pattern, per capita built mass declines as cities get bigger (by definition of 'per capita', $\beta = 0.9 - 1 = -0.1$; Fig. 2b inset): a tenfold-larger city carries only ~80% of the mass per resident. Per capita mass is therefore a poor metric for comparing cities of different sizes (dashed black vs orange line, Fig. 2b).

The scale-induced efficiencies can largely be attributed to the shared use of infrastructure in larger urban areas. As cities grow, they facilitate the communal utilization of resources such as roads, utilities and public spaces, leading to economies of scale that reduce the per capita built mass. This phenomenon aligns with the concept of urbanization economies[22], where the concentration of population and activities in urban centers enhances productivity and resource efficiency through shared infrastructure and services. These findings extend previous studies on urban scaling[7,23], which demonstrated that the lengths of infrastructure (roads, cables and pipes) scale sublinearly with population due to the increasing efficiency of spatial connectivity in larger urban systems.

However, previous studies have largely focused on the geometry (for example, length or area) of infrastructure rather than its material embodiment. Our analysis introduces a new dimension: the total mass of the built environment, which offers a more direct account of the material and energetic investments embedded in infrastructure that is directly relevant to material projections.

Whereas these results underscore the universality of sublinear scaling at the city level, they prompt further inquiry into whether similar patterns hold within cities themselves. Despite recognition of cities displaying self-similar features at various spatial scales, previous efforts of urban scaling analysis have often assumed cities to be homogenous (for example, per capita projections). This homogeneity assumption treats cities as internally uniform: neighborhoods resemble one another in population density and built environment. Real urban areas, by contrast, are diverse and uneven. In the next section, we challenge this homogeneity assumption by examining how built mass scales with population at the level of neighborhoods.

Stronger economies of scale at the neighborhood level

Neighborhoods are fundamental units of human settlement, shaping daily life, economic opportunity and urban form from ancient times to the present. Urban sociologists have long highlighted their importance[24] neighborhoods remain underrepresented in urban scaling analyses, largely because most studies take whole cities as the unit and lack the high-resolution spatial data needed to analyze intra-city variation. In this paper, we define neighborhoods (population n and built mass m) using a global hexagonal grid (H3 Resolution 6, ~3.7 km

https://doi.org/10.1038/s44284-026-00532-x

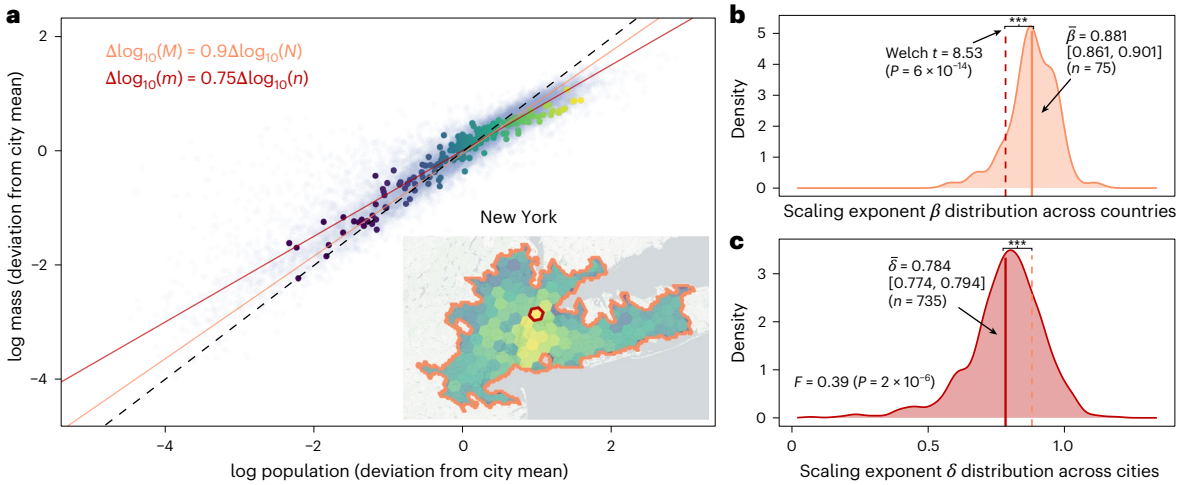


Fig. 3 | Sublinear scaling of built mass across neighborhoods. a, Scatter plot of the centered log total built mass versus centered log population, with regression lines showing the across-neighborhood scaling relationship (red, slope $\delta = 0.75$, confidence interval [0.747, 0.754]; $n = 17{,}497$; $R^2 = 0.89$) and the across-city relationship (orange, slope $\beta = 0.9$). The dashed black line indicates linear scaling (slope = 1). Colored points highlight neighborhoods in New York, with an inset hex map showing their spatial distribution of population. Boxplots show the fitted slopes. Note that all neighborhoods in our dataset are lumped together after centering. **b**,**c**, The distribution of city scaling exponents across 75 countries (≥5 cities) indicating β has a symmetrical distribution around 0.88 (confidence interval [0.86,0.90]). Similarly, neighborhood scaling exponent across 735 cities (country ≥5 cities; city ≥10 neighborhoods) reveals a mean of $\delta = 0.78$ (confidence interval [0.77, 0.79]). According to the two-sided F test, the variance of the two distributions are significantly different ($F = 0.39$, $p = 2e{-}6$; $^{***}P < 0.001$) and a subsequent two-sided Welch t test confirms that the difference between β and δ is statistically significant ($t = 8.53$, $p = 6e{-}14$). Map data in **a** © OpenStreetMap (https://www.openstreetmap.org/copyright). Position basemap tiles from CARTO under a Creative Commons license CC BY 3.0.

center-to-corner radius; Methods) at a spatial scale that captures the extent of day-to-day human activity.

Across a global dataset of urban neighborhoods, we observe that built material mass increases sublinearly with population in both across-city ($M = M_0 N^{\beta}$) and across-neighborhood ($m = m_0 n^{\delta}$) comparisons. Importantly, because each neighborhood polygon in our sample has nearly the same land area, its 'population n' can be considered a measure of density—unlike whole-city population size N, which combines density and total area. We apply the same centered-scaling method, centering each neighborhood's log(population) and log(mass) by their means. This yields a markedly lower scaling exponent within cities ($\delta = 0.75$ confidence interval [0.747, 0.754]; red line, Fig. 3a) than across cities ($\beta = 0.90$ confidence interval [0.89,0.91]; orange line). In other words, local density effects within a city generate even more pronounced economies of scale than aggregate city-to-city comparisons.

Consistent with the city-level analysis, this result is robust to the choice of underlying datasets, repeated analysis using independent sources or their mixtures yield δ values between 0.728 and 0.776 (Supplementary Table 7). The neighborhood scaling exponent is consistently sublinear whether neighborhoods are drawn one step coarser or finer than our primary 3.7-km-radius H3 grid ($\delta = 0.83$ at ~9.9 km, 0.75 at ~3.7 km and 0.71 at ~1.4 km radius; H3 grid resolutions 5, 6 and 7; Supplementary Fig. 1). It is also insensitive to H3 grid placement (maximum δ deviation of 0.017 across four cardinal shifts; Supplementary Table 8). In summary, across all dataset sensitivity combinations neighborhood scaling exponent (δ) is consistently more sublinear than city-level exponent ($\beta - \delta > 0$), pointing to stronger economies of scale at the neighborhood level.

Beyond the lump-sum aggregate analysis of Fig. 3a, we also reveal a curious and systematic difference in variance of slope when we analyzed β across individual countries and δ across individual cities (Fig. 3b,c). In particular, the variance of δ across 735 unique cities is significantly higher than the variance of β across 75 countries meeting our selection criteria (F test, $F = 0.39$, $p = 2e{-}06$). This corroborates prior findings that smaller spatial units tend to show more noise[25].

Our findings expand upon and unify several strands of recent research. Prior studies[17,26] have found lower per capita mobility infrastructure mass in denser urban areas. Other research[9] similarly indicates that total built mass per capita is lower in denser urban settings but without systematically quantifying these relationships. Sublinear scaling patterns for building volumes have been identified within ten individual Chinese cities[27], but the study is geographically limited, raising the question of global generalizability. Our analysis addresses this gap by demonstrating a universal sublinear scaling trend in total built mass at the neighborhood level across thousands of cities worldwide.

Three mechanisms underpin these neighborhood-level economies of scale. First, vertical densification concentrates residents: taller buildings in denser areas[28] share foundations, roofs and structural cores across more dwelling units, lowering per capita material use. Second, dwellers in denser areas functionally trade private living space (for example, home gym, private garage, home kitchen, private study room) with shared public amenities (for example, commercial gym, restaurants, public library), effectively reducing per capita space demand for a given level of utility[29]. Third, denser settlements serve more residents per unit of road network, so network mass grows more slowly than population[7]. The strength of all these mechanisms depends on how much daily activity stays within a neighborhood. Applying the truncated power-law displacement model[30] to our hexagon grids, we estimate that residents spend approximately 89% of their trips within a 3.7-km radius. This matches the edge length of our neighborhood hexagons (Supplementary Notes 4 and 5). The majority of social interactions occur locally, enabling residents to share network infrastructure and amenities and thereby achieve higher material efficiency.

These mechanisms in theory should be agnostic of the granularity of spatial units. This raises a key question: why does the scaling exponent increase when moving from local ($\delta = 0.75$) to aggregate scales ($\beta = 0.9$) and what mechanisms can bridge these levels?

Emergence of across-city sublinear scaling from across-neighborhood disparity

Bigger cities tend to develop denser neighborhoods because agglomeration effects drive up land values, creating strong incentives to build upward and cluster people together to maximize the benefits.

If all residents in bigger cities were concentrated in denser neighborhoods—leveraging those steep economies of scale—the city-level scaling could approach 0.75. But in reality, even large cities mix low- and high-density areas, so not all population benefits equally from density-induced efficiencies, pushing the aggregate β higher. The unevenness of within-city population distribution probably determines how much neighborhood-level savings 'trickle up' to shape city-wide patterns.

We thus hypothesize that the degree of population heterogeneity is the key that bridges scaling across the two nested spatial scales: across cities ($\beta = 0.90$) and across neighborhoods ($\delta = 0.75$). Existing research suggests that neighborhood populations often conform to Zipf-like, heavy-tailed distributions, where a small number of dense neighborhoods house disproportionately larger amounts of residents[25,31]. Given the sublinear scaling of built mass at the neighborhood level, these dense areas benefit from enhanced economies of scale, reducing the per capita built mass at the city-wide level.

To test this hypothesis, we developed a theoretical model comprising simulated cities with neighborhoods whose populations follow a Zipf-like distribution described by an across-neighborhood disparity parameter s (Methods). Per city distribution testing confirms that Zipf-like distributions are strongly preferred over log-normal alternatives: among 633 cities with sufficient sample sizes, Zipf is significantly favored in 22% of cities vs. <1% for log-normal (Vuong likelihood ratio test; Supplementary Table 9). In this set-up, the population of the ith ranked neighborhood is $1/i^s$ of the largest neighborhood: populations are more concentrated in denser neighborhoods in cities with larger s (Fig. 4a inset). Neighborhood-level built mass was assigned using the empirical scaling exponent ($\delta = 0.75$), then aggregated to obtain total city-level built mass (M) and population (N). We estimated the across-city scaling exponent β by regressing $\log(M)$ against $\log(N)$ across these simulated cities. We introduced two random processes to capture the variability: (1) we drew a random s parameter from a normal distribution, centered at the given s with a standard deviation (0.59) estimated from the observed distribution (Fig. 4a); (2) we grouped the cities randomly into 'countries' and conducted separate regressions, producing a distribution of theoretical β values.

We found that the observed distribution of the disparity parameter s is right skewed (Fig. 4a), which suggests that a small number of cities have very heterogeneous neighborhoods (that is, coexistence of very dense and very sparse neighborhoods). On the basis of the observed distribution of s (mean = 1.16, standard deviation = 0.59), we simulated across-city scaling exponents (β), which strongly aligns with observed exponents (Fig. 4b). By sweeping values of s, our simulations map how neighborhood disparity s influences city-level scaling exponent β, depicting a smoothly declining curve from nearly linear ($\beta \approx 1.0$) at low disparity to strongly sublinear (β approaching $\delta = 0.75$) at high disparity (Fig. 4c). Our mathematical derivation (Methods) further shows that across-city scaling exponent β is intrinsically bounded by two limits ($\delta \le \beta \le 1$), explaining the increase of exponent when moving from local (neighborhood) to the aggregate (city).

Our empirical analysis and theoretical simulations indicate that within-city density disparities are a critical mechanism underpinning economies of scale in built material use. Denser neighborhoods, often housing a disproportionate share of the urban population, require less built mass per capita; thereby driving the sublinear scaling observed at the city level. Classical urban economic models[32] provide a well-established explanation for the emergence of these disparities. In monocentric cities, proximity to the central business district raises land values and incentivizes denser development near the core. In polycentric cities, multiple subcenters generate additional peaks of accessibility and land value, sustaining density gradients as households and firms cluster around these nodes[33].

However, zoning regulations and density constraints can suppress this natural tendency towards concentrated development[34]. Restrictions such as maximum floor-area ratios, height limits or exclusionary zoning limit high-density construction in areas with strong market demand, effectively flattening the urban density gradient (artificially decreasing s and increasing β). As a result, such anti-density interventions may unintentionally erode the material efficiency gains associated with urban density variation and consequently undermine the very mechanism that enables cities to use built materials more efficiently.

Cities as nested complex systems of built structure

Our analysis indicates that conventional per capita projections systematically overestimate the required built mass in larger cities and denser neighborhoods. According to the latest Intergovernmental Panel on Climate Change (IPCC) assessment report[35], cement and steel—critical materials primarily used for built mass—account for ~5.2 Gt carbon dioxide equivalent (CO_2-eq) yr^{-1} of global emissions. From 2018 to 2050, the cumulative buildings, infrastructure and machinery-related emissions are projected[4] to reach between 1,300 and 2,100 $GtCO_2$-eq, driven mainly by increasing material stocks. Yet these projections treat every future urban resident as if they would require the same amount of material irrespective of the size or form of the city they live in.

Neglecting size-dependent nonlinear scaling may lead to substantial mis-estimations in material demand—an issue illustrated when re-examining a recent UN-Habitat projection[36] through the lens of our findings. This projection shows that in low-income countries, the population living in megacities ($N > 5$ millions) will rise from 18 million today to about 140 million by 2070. In those countries, the projected future population living in megacities will be roughly equal to the population (~160 M) that now inhabit small cities ($N < 250$k). According to the across-city scaling relationship revealed here ($\beta = 0.9$), a city with population size 20-fold of another (5 M vs 250k) merely demands material stock that is about 15-fold ($20^{\beta} \approx 14.8$). This means that accommodating the same number of people in megacities, instead of small cities, is associated with a roughly 26% lower per capita material stock ($1 - 14.8/20 \approx 0.26$).

We do need to caution that cross-sectional association (Figs. 2 and 3; as opposed to longitudinal) is not causal and does not necessarily predict how individual cities will evolve as they grow; even a first-order projection would hold only if, for example, migrants keep settling according to current patterns. Built-stock accumulation also depends on income growth, technology change and policy choices. With the rising availability of high-resolution chronosequence urban data, future analysis might be able to reconstruct the 'ontogenetic growth' of cities, better elucidating the changing material efficiencies as cities grow bigger. Regardless, our analysis does point to the possibility that capping city size may artificially restrict an important venue of material-efficiency gain.

Within cities, we find a steeper sub-linear scaling of built mass with population density ($\delta = 0.75$, by definition 'per capita' scaling coefficient is $0.75 - 1 = -0.25$). Unfortunately, existing scenario studies[36,37] stop at country-level averages and cannot tell us how many people will live in very-high- or very-low-density neighborhoods. For example, in one potential scenario, UN-Habitat projections[36] suggest that average urban density in low-income countries could increase to 164% of current levels by 2050. If this happens, and we apply our scaling exponent ($\delta = 0.75$), the per capita built mass in a neighborhood would be associated with a 12% reduction ($1.64^{-0.25} = 0.88$) compared to linear projections. However, this average-density scenario still overlooks the heterogeneous nonlinear effects across various neighborhoods. Moreover, our cross-sectional results reflect statistical associations observed now, not deterministic predictions of temporal trajectories. Nevertheless, future projections must shift from average densities to distributions among multiple density levels if we are to understand the real material stakes of urban growth.

Beyond material efficiency, urban scale and density also lead to notable socioeconomic advantage. Large cities enable deeper labor

https://doi.org/10.1038/s44284-026-00532-x

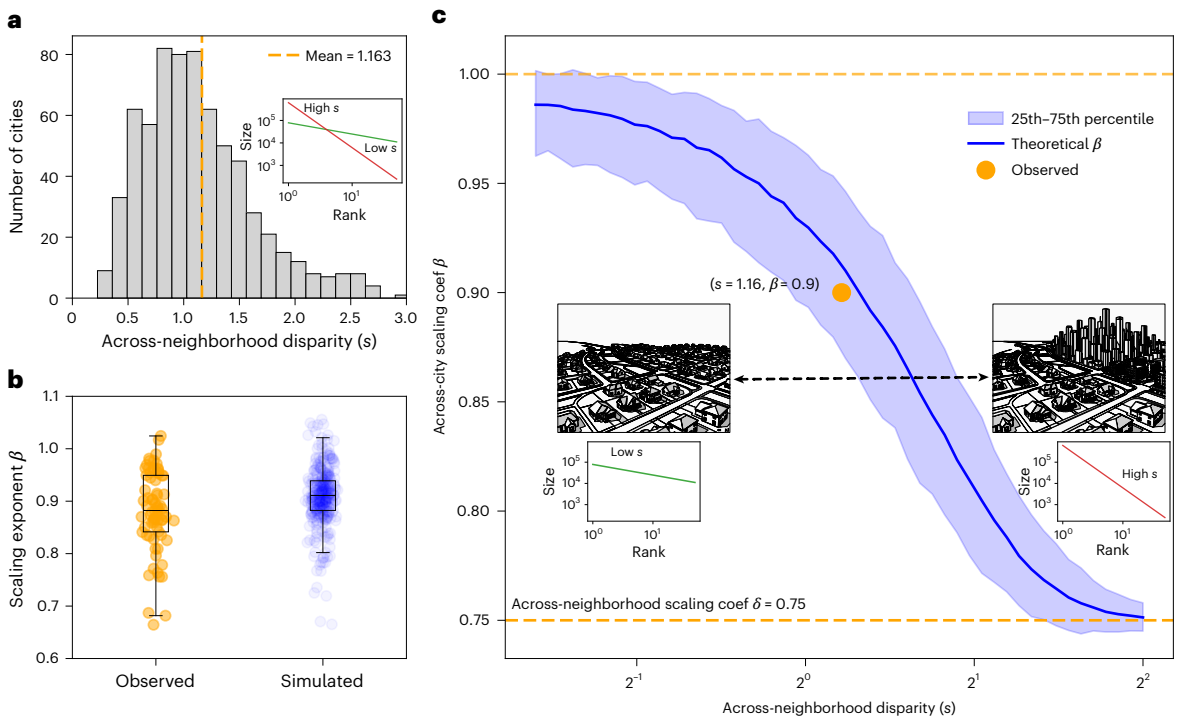


Fig. 4 | Emergence of sublinear across-city scaling from across-neighborhood disparity. The disparity parameter *s* (Zipf's exponent) captures how uneven population is distributed across neighborhoods—larger *s* indicates greater disparity (a few dense neighborhoods dominate), while smaller *s* reflects more uniform distributions. **a**, Probability distribution of *s* across cities, with the mean (*s* = 1.16) marked by a dashed line. Insert plot illustrates the rank-size distributions of cities with high and low *s* values. **b**, Boxplots comparing observed city-level scaling exponents *β* (orange, *n* = 75) with those predicted by theoretical simulations (blue, *n* = 143), showing strong agreement. Simulated cities assume Zipf-like neighborhood population distributions and a fixed within-city scaling exponent (*δ* = 0.75). In each box plot, the lower and upper bounds of the whiskers denote minima and maxima, the center line denotes the median and the lower and upper bounds of the boxes represent the 25% and 75% quantiles, respectively. **c**, Theoretical relationship between *s* and *β* (both scaling coefficient labeled as 'scaling coef'; solid blue line denoting the mean while shaded band the 25th–75th percentile interquartile range): a system of more homogenous cities (illustration showing cities with uniform single family housing districts, small *s*) approaches linear scaling (upper bound, *β* ≈ 1), while a system of more heterogeneous cities (illustration showing cities with buildings of varying heights, large *s*) converges toward the within-city exponent (lower bound, *δ* = 0.75). The empirical means (*s* = 1.16, *β* = 0.90, orange point) align with this trend. Credit: illustrations in **c**, Liang Chen.

market pooling, specialized supplier networks and extensive knowledge sharing, all of which bolster innovation and productivity[38]. For instance, a bigger urban population allows a finer division of labor and supports niche industries and services that require a broad customer base, which tend to cluster in major cities[39]. In fact, even a tiny fraction of people with a niche interest can form a critical mass in a metropolis[40]. High population density further reduces the spatial separation between people and opportunities, facilitating efficient matching in the labor market and easy access to specialized services[41]. Dense neighborhoods also promote more frequent face-to-face interactions and serendipitous encounters—the 'unplanned synergies' that have been widely recognized in urban studies[42–44] as drivers of innovation and social connectivity. Together, these mechanisms suggest that urban scale and density are key drivers of social and economic opportunities, providing access to spatialized markets, services and social networks that less dense or smaller urban areas cannot easily support.

Whereas increasing city sizes and neighborhood densities can enhance material efficiency and bring socioeconomic advantages, unchecked growth and densification can intensify social and public health challenges. For instance, larger cities often experience disproportionate increases in congestion, crime and infectious diseases, as these outcomes scale superlinearly with population size, reflecting the complex dynamics of urban environments[45–47]. Moreover, in densely populated urban slums, shared sanitation facilities are prevalent due to limited space and resources, but poor maintenance and hygiene often lead to health risks and diminished quality of life[48]. The collective responsibility for maintaining such facilities frequently results in neglect, as individuals are less motivated to care for shared spaces. These challenges highlight the need to balance material efficiency with investments in infrastructure that ensure adequate living standards[49] and public health in high-density urban areas.

Taken together, our findings collectively establish the importance to recognize these linked, multi-scale material implications as intrinsic properties of cities. Viewing cities as complex adaptive systems, whose performance depends jointly on their overall size and their hierarchically nested internal structure[50], will enable more holistic and effective policy interventions in the pursuit of a more productive, equitable and sustainable urban future.

Methods

Historical trend of global built structure mass

We derived historical global population data from Our World in Data (https://ourworldindata.org/grapher/population). We acquired the global built structure mass and global biomass dataset from Elhacham et al.[2] (source data from ref. 51) from 1900 to 2015 and projection data from 2015 to 2037[2]. We used linear interpolation (zoo::na.approx()) to interpolate missing global biomass value during 1991–1999, 2001–2009, 2011, 2013–2016. To calculate the built structure to human mass ratio, we estimated weighted average human body mass as approximately 50 kg. We derived this coarse-grained estimation by combining the global average age distribution (25% 0–14, 65% 15-–64, 10% 65+ in year 2023 based on World Bank data, https://data.worldbank.org/indicator/SP.POP.0014.TO.ZS) with the age-specific body mass (25 kg for 0–14, 60 kg for 15–64, 50 kg for 65+). Age-specific body mass varies

across countries and diets, but our qualitative conclusions are not sensitive to this estimation.

Vegetation biomass

We extracted city-specific vegetation biomass from a recently published global map of vegetation carbon that includes both aboveground and belowground biomass carbon[52]. The vegetation carbon data is based on 2010. We then converted biomass carbon into dry-weight vegetation biomass using a conversion coefficient of 0.48 g carbon per gram of dry-weight biomass[53]. We extracted city-specific vegetation biomass based on city definitions described in the following section.

Definition of cities

In this study, we define cities using the concept of Urban Cores provided by the Global Human Settlement Layer. Global Human Settlement Layer, developed by the European Commission's Joint Research Centre, delineates urban cores based on continuous areas of built-up land and population density, derived from satellite imagery and census data[16]. An urban core is typically characterized by contiguous built-up surfaces with high population density, representing the primary agglomeration of urban activity within a region. Following established conventions, we include only cities with a minimum population size of 50,000 residents in our analysis, ensuring consistency and comparability with other global urban studies[3,8]. Our main finding that economies of scale in urban built stock are prevalent in cities worldwide is robust to the arbitrary cut-off sizes of cities.

Definition of neighborhoods

We delineate neighborhoods with the H3 global hexagonal grid (developed by Uber)[54]. Hexagons have two properties that are critical for our analysis. First, among the few regular polygons that tessellate the plane, hexagons minimize the perimeter-to-area ratio, yielding compact, near-circular units that reduce edge effects when we aggregate spatial data. Second, hexagons tile space without the directional bias that characterizes squares (Manhattan effect) or triangles, thereby supporting isotropic distance measures that better approximate real-world movement patterns. These features mirror the intuition of Christaller's central-place theory[55], which idealizes market areas as a nested hierarchy of hexagons to maximize coverage while minimizing overlap. Here we use the hexagons at resolution of level-6, where each cell has an average edge length of ~3.7 km and an area of ~36 km^2, a scale that captures the extent of day-to-day human activity: the cell radius can be covered in ~15 min by bicycle (15 km h^{-1}) or ~45 min on foot (5 km h^{-1}), and residents spend approximately 89% of their trips within the focal hexagon[30]. The resulting neighborhoods are therefore large enough to encompass the functional mix of a self-contained urban district, yet fine-grained enough to retain intra-city variation in the variables we study. Sensitivity analyses at coarser and finer resolutions (levels 5 and 7) are provided in Supplementary Note 4.

Bottom-up approach of urban built stock

To quantify the material stocks embedded in the built environment of cities, we devised a workflow that builds up the total mass of urban buildings and paved surfaces from the ground up. This method separately estimates the volumes of buildings and areas of mobility infrastructure within each city boundary and relies on well-established, type-specific and region-specific material-intensity factors to convert built volume, road surface and pavements into mass, detailed below.

Stock of buildings. We use raster-based estimates of building volume provided independently by Esch et al.[13], Li et al.[11] and Liu et al.[12], which offer 3D characterizations of urban form at various spatial resolutions (Supplementary Table 1). To minimize dataset-specific bias, we calculate the average building volume within each city boundary using all three datasets (Extended Data Figs. 2–4).

We then converted building volume to built-stock mass using a detailed material-intensity framework that considers both (1) building types and (2) regional construction practices developed by Haberl et al. for analyzing global buildings[18]. We distinguish building types based on Global Human Settlement Layer settlement characteristics (GHS-BUILT-C) classifications, as the distinct function and form of different building types demands different building standards and consequently different material intensities independent of country and region. Similarly, material intensity is also a function of country and region due to the dependence of building on local climate, building practices, developmental level and so on. In Supplementary Table 2, we provide a summary look-up table for matching building types to material intensities. For the detailed regional breakdown (Organisation for Economic Co-operation and Development (OECD), North America, Japan, China and so on), please refer to Haberl et al.[18] Extended Table 5.

Stock of mobility infrastructure and other pavement. For impervious surface data, we use the Global Impervious Surface Area (GISA-10m) product from Huang et al.[15], which maps global impervious cover at 10-meter resolution. To isolate the portion of impervious surface attributable to pavement (for example, roads, sidewalks), we subtract the building footprint area—estimated from the previous step by averaging Li et al.[11], Liu et al.[12] and Esch et al.[13]—from the total impervious surface within each city.

After extracting pavement area, we further tease out five grades of roads network vs other pavements (sidewalks, parking lot) given the big difference in their required structural intensity and consequently material intensity. For each city, we calculate the total length and total area of the road network per road grade: with decreasing material intensity, highway, primary, secondary, tertiary and local (road network source: Global Roads Inventory Project (GRIP), ref. 14). We then convert road area to road stock mass based on a type-specific and region-specific material intensity look-up table (summarized in Supplementary Table 3, full table uploaded as separate supplementary file, derived from ref. 17).

For other pavements (for example, sidewalks, parking lots), we assume a material intensity of 570 kg m^{-2} (equivalent to about 20 cm of concrete or asphalt), a value lower than typical road material intensity adopted by previous meta-analysis in the field of industrial ecology (Frantz et al. Extended Data Table 15 for parking lots[9]).

Subway/metro infrastructure evades remote sensing; we estimated its mass from compiled network geometries (China Public Transport Operation Network Dataset (CPTOND-2025) for China; OpenStreetMap elsewhere) using per kilometer tunnel and per station coefficients from Mao et al.[56]. Subway mass is included in city totals (Fig. 1), whereas scaling baselines comprise the remotely sensed aboveground stock; subway inclusion is evaluated using sensitivity analysis, which shifts the scaling exponents negligibly ($\Delta\beta = +0.003$, $\Delta\delta = +0.001$; Supplementary Note 3).

The total mass of urban built stock is the sum of the estimated building, road mass, other pavement and subway mass.

Since we completed our analysis, more recent and more comprehensive global estimates of mobility infrastructure stocks have become available, notably Total Resources in Physical Infrastructure (TRIPI)[57] and Wiedenhofer et al.[26]. These new estimates report larger absolute totals than earlier estimates[17], mainly because they span the entire global network and additional infrastructure classes (for example, rail) rather than the within-city pavement analyzed here. We retain ref. 17 as our source of per area material intensities; TRIPI also adopts these same intensities for paved roads, so our coefficients remain consistent with the most recent work. Our pavement area, separately, is measured directly from impervious surface remote sensing rather than inferred from mapped road lengths, so incomplete network coverage is unlikely to reduce our estimated pavement mass.

Data acquisition for urban population

We used the WorldPop dataset to calculate the total population of each city by summing pixels within city boundaries from WorldPop raster datasets. We chose WorldPop due to its high spatial resolution (100 m), detailed demographic representation, frequent updates and open accessibility[58,59].

Scaling theory and centered-scaling analysis

Scaling theory studies the change of system properties as a system changes in its size[60]. Its conceptual foundation can at least be traced back to early insight regarding proportional scaling up (that is, linear scaling) built infrastructure in Galileo's *Two New Sciences*[61]. Galileo deducted that scaling structures proportionally in size increases their volume and mass at a faster rate than the increase of strength, leading to structural failures. Mathematically, this type of relationship is expressed through power-law equations of the general form:

$$Y = Y_0 N^{\beta}$$

In this equation, Y denotes a measurable property or characteristic of the system, N represents system size, β is the scaling exponent capturing how quickly a property changes relative to system size and Y_0 is the normalization constant, representing the elevation of the scaling relationship on a log–log plot[62,63], providing insights into the baseline or developmental level of the system (for example, a collection of buildings, a taxon of multiple species or a group of cities).

Aside from its widespread application in physics and engineering, scaling theory greatly influenced biology through the early twentieth century subfield of allometric analysis, enhancing the adoption and interpretation of Darwin's evolutionary theory[64–67]. Notable examples include scaling relationships such as organism body mass with metabolic rate and tree height with stem diameter. These foundational biological concepts were further expanded by West, Brown and Enquist, who formalized biological scaling laws, laying the groundwork for applications in other complex systems, including urban contexts initiated by Bettencourt and colleagues[23].

Scaling theory has recently been widely adopted to enhance our understanding of urban systems, elucidating how a wide range of urban indicators (wealth, innovation, crime, infrastructure, waste and so on) scale with city population size[8,68]. Variations in the exponent indicate critical nonlinearities—economies or diseconomies of scale—that are often obscured by simple per capita measures. Superlinear scaling ($\beta > 1$) characterizes intensified social interactions and innovation typically seen in larger cities, whereas sublinear scaling ($\beta < 1$) describes constraints related to physical infrastructure and spatial limits[7].

To statistically manage correlations between the scaling exponent β and normalization constant Y_0, the method of fixing slope and estimating elevation is commonly applied, originating from biological analyses[62,69,70]. In the context of our analyses, the main focal point is on the scaling slope. We thus adopted an even more straightforward approach of centered scaling developed by Bettencourt and Lobo[20] where we center the data by subtracting the average log of population and the average log of mass in each dimension, effectively removing the effect of intercept (intercept = 0) on slope during regression. We use this statistical approach to derive the general scaling relationship between city mass and population by removing the effect of country-specific baseline differences and the general neighborhood scaling by likewise removing city-specific baseline differences.

Sensitivity analysis

To assess the robustness of our scaling exponents, we conducted four sensitivity analyses examining key sources of methodological uncertainty. First, we tested how building volume data source choice affects results by repeating analyses using three independent global datasets[11–13] individually, in random combinations and weighted by regional validation accuracy (Supplementary Table 4). Second, we evaluated whether regional variation in material-intensity assumptions influences scaling patterns by comparing three frameworks: a single global average, a five-region classification[18] and a fine-grained 32-region classification accounting for climate and development stage[71]. Third, we quantified the potential impact of underground infrastructure—absent from our baseline estimates—by incorporating subway network data[56] and bounding the contribution of other buried utilities using high-resolution US material-stock assessments[9] (Supplementary Note 3 and Supplementary Table 11). Fourth, we examined whether neighborhood delineation affects within-city scaling by analyzing three hexagonal grid resolutions (H3 levels 5, 6 and 7) and by displacing the grid in cardinal directions.

Across all sensitivity tests, scaling exponents remain robustly sublinear, with variation from any single methodological choice roughly an order of magnitude smaller than the deviation of β and δ from unity. Detailed methods, results and figures are provided in Supplementary Notes 1–4 (Supplementary Tables 4–11).

Simulation of the emergence of across-city scaling from across-neighborhood disparity

We developed a simulation framework to investigate how variations in the neighborhood-level Zipf's law distribution of population (characterized by the Zipf shape parameter s) influence city-level scaling patterns, given a fixed neighborhood-level scaling exponent ($\delta = 0.75$). The total built mass (M) of cities was modeled as the sum of neighborhood-level built masses (m_i), where $m_i = n_i^{\delta}$ and n_i is the population of the ith neighborhood. With these simulated cities, we then estimated the scaling coefficient (β) relating M to N using log–log regression.

To explore the emergent relationship between s and β, we performed a parameter sweep of s values and analyzed the city-level scaling patterns across a range of scenarios. This approach revealed how the aggregation of neighborhood-level power-law distributions affects the observed scaling exponent at the city level. To examine the uncertainties of β, we introduced two random processes: (1) we drew a random s parameter from a normal distribution, centered at the given s with the standard deviation (0.59) estimated from the observed distribution (Fig. 3a inset and Fig. 4a); (2) we grouped the cities randomly into 'countries' by Dirichlet distribution with shape parameter of 0.1 to generate a power-law-like distributions of countries ranked by numbers of cities. By applying these two random processes, we produce a distribution of theoretical β values.

Derivation of across-city scaling law from across-neighborhood disparity

We partition each city into K standard hexagonal neighborhoods. Let n be the population of a neighborhood and m be its built mass. Following the statistical framework of urban indicators developed by Gomez-Lievano et al.[25], we treat both population and built mass as stochastic variables to account for the intrinsic noise and fluctuations of urban population and infrastructure. Empirical evidence suggests that these quantities are highly right skewed and can be characterized by heavy-tailed probability distributions. Per city distribution testing following Clauset, Shalizi and Newman[72] shows that Zipf-like distributions are strongly preferred over log-normal alternatives (Vuong likelihood ratio test; Supplementary Note 6 and Supplementary Table 9).

We characterize these distributions as Pareto Type I: $P(n) \propto n^{-\alpha_n}$ and $P(m) \propto m^{-\alpha_m}$, where α_n and α_m are tail exponents. The Pareto distribution (continuous density) and Zipf's law (discrete rank size) are equivalent representations linked by $\alpha = 1 + \frac{1}{s}$. We use Zipf's law for empirical estimation and the Pareto form for analytic derivation. The tail exponent α encodes intra-city disparity: a homogeneous city corresponds to $s \to 0$ and $\alpha \to \infty$, whereas greater disparity corresponds to larger s and smaller α, bounded below by 1 for normalizability (Fig. 4). The tail exponents are thus estimated as $\alpha_n = 1 + \frac{1}{s_n}$ and $\alpha_m = 1 + \frac{1}{s_m}$.

Instead of assuming a deterministic one-to-one mapping between the rank of a neighborhood's population and the rank of its built mass, we link these variables using conditional probability. Because the accumulation of urban infrastructure is impacted by population-dependent, multiplicative social interactions, the conditional probability of built mass given population, $P(m|n)$, is best described by a log-normal distribution[25]. The scaling relationship at the neighborhood level thus emerges as the expectation value of this conditional probability: $\langle m|n\rangle \propto n^{\delta}$ where δ is the neighborhood-level scaling exponent.

By the law of total probability, the marginal distribution of built mass, $P(m)$, can be obtained by integrating the joint probability over all possible values of population n: $P(m) = \int_0^{\infty} P(m|n)P(n)\mathrm{d}n$.

As demonstrated by Gomez–Lievano et al.[25], marginalizing the log-normal conditional probability over the heavy-tailed distribution of population mandates an exact mathematical constraint between the scaling exponent (δ) and the probability distribution exponents (α_n, α_m): $\delta = \frac{\alpha_n - 1}{\alpha_m - 1}$.

Substituting our Zipf rank parameters into this exact marginalization result mathematically bridges the statistical distributions back to our rank-order variables: $\delta = \frac{(1+1/s_n)-1}{(1+1/s_m)-1} = \frac{1/s_n}{1/s_m} = \frac{s_m}{s_n}$.

If $s_m < s_n$, then $\delta < 1$, implying a sublinear growth of expected built mass with population. In our dataset, s_m is consistently smaller than s_n, indicating that the distribution of neighborhood-level mass is more homogeneous than the distribution of neighborhood-level population.

We then define the total city population (N) and total city built mass (M) as the sum across all K neighborhoods: $N = \sum_{i=1}^{K} n_i$, $M = \sum_{i=1}^{K} m_i$.

Assuming $m_i \propto n_i^{\delta}$, we can deduce how the city-level scaling exponent (β), where $M \propto N^{\beta}$, is bounded. If $s_n \gg 1$ and $s_m \gg 1$, the system is in a highly disparate regime where the largest neighborhood dominates the total sums. In this case: $N \approx n_{(1)}$, $M \approx m_{(1)} \propto (n_{(1)})^{\delta}$, therefore $M \propto N^{\delta} \Longrightarrow \beta = \delta$.

Conversely, if s_n and s_m are close to zero, the neighborhoods are nearly identical in size, placing the system in a homogeneous regime. In this case: $N \propto K$, $M \propto K$, therefore $M \propto N \Longrightarrow \beta = 1$.

Hence the city-level scaling exponent β is theoretically bounded between δ (in a largest-neighborhood-dominated regime) and 1 (in a highly homogeneous regime).

Statistical analyses

We used linear regression to analyze the relationship between city mass and urban population (Fig. 2a,b and Extended Data Figs. 5 and 6; lm, R package 'stats', v.4.4.0). Both variables are right skewed and were log10 transformed before analysis, consistent with logarithmic scale presentation of our figure axes. For Fig. 2b, we isolate the universal scaling relationship by removing country-level baseline differences through de-centering[20]. For each country, we compute the country c mean of log population and log mass across its cities, then subtract these means from each city's values:

$$\Delta \log M_i = \log M_i - \underline{\log M}_c\,,\ \Delta \log N_i = \log N_i - \underline{\log N}_c$$

We then regress the pooled de-centered log mass on the de-centered log population by ordinary least squares. By construction the intercept is zero, and the slope β captures the universal elasticity of city-level built mass with respect to population, net of cross-country differences in construction norms, material availability and development history. For Fig. 3, the same within-group de-centering is applied one level deeper. For each city j, we subtract the city-level means from each neighborhood's log population and log mass:

$$\Delta \log m_{jk} = \log m_{jk} - \underline{\log M}_j,\ \Delta \log n_{jk} = \log n_{jk} - \underline{\log n}_j$$

Ordinary least squares on the pooled de-centered neighborhood data yields the within-city elasticity δ, which captures how built mass scales with population across neighborhoods of the same city.

We include only cities with total population > 50,000 and ≥ 10 qualifying H3 hexagons (resolution 6, ~36 km^2) and only countries with ≥ five qualifying cities. All analyses were conducted in R (v.4.4.0).

Reporting summary

Further information on research design is available in the Nature Portfolio Reporting Summary linked to this article.

Data availability

All data supporting the findings of this study are publicly available via figshare at https://doi.org/10.6084/m9.figshare.29482190 (ref. 73). An interactive visualization of these global mass patterns is also provided online (https://city-mass.nested-complexity.net).

Code availability

All code used to produce the findings of this study is publicly available via figshare at https://doi.org/10.6084/m9.figshare.29482190 (ref. 73).

References

1. Krausmann, F. et al. Global socioeconomic material stocks rise 23-fold over the 20th century and require half of annual resource use. *Proc. Natl Acad. Sci. USA* **114**, 1880–1885 (2017).
2. Elhacham, E., Ben-Uri, L., Grozovski, J., Bar-On, Y. M. & Milo, R. Global human-made mass exceeds all living biomass. *Nature* **588**, 442–444 (2020).
3. Cattaneo, A. et al. Worldwide delineation of multi-tier city–regions. *Nat. Cities* **1**, 469–479 (2024).
4. Krausmann, F., Wiedenhofer, D. & Haberl, H. Growing stocks of buildings, infrastructures and machinery as key challenge for compliance with climate targets. *Glob. Environ. Change* **61**, 102034 (2020).
5. United Nations Publications *World Urbanization Prospects: The 2018 Revision* (UN, 2019).
6. Swilling, M. et al. *The Weight of Cities: Resource Requirements of Future Urbanization* (UN Environment International Resource Panel, 2018).
7. Bettencourt, L. M. A. The origins of scaling in cities. *Science* **340**, 1438–1441 (2013).
8. Lu, M., Zhou, C., Wang, C., Jackson, R. B. & Kempes, C. P. Worldwide scaling of waste generation in urban systems. *Nat. Cities* **1**, 126–135 (2024).
9. Frantz, D. et al. Unveiling patterns in human dominated landscapes through mapping the mass of US built structures. *Nat. Commun.* **14**, 8014 (2023).
10. Bettencourt, L. M. A. & Marchio, N. Infrastructure deficits and informal settlements in sub-Saharan Africa. *Nature* **645**, 399–406 (2025).
11. Li, M., Wang, Y., Rosier, J. F., Verburg, P. H. & van Vliet, J. Global maps of 3D built-up patterns for urban morphological analysis. *Int. J. Appl. Earth Obs. Geoinf.* **114**, 103048 (2022).
12. Liu, X. et al. Global mapping of three-dimensional (3D) urban structures reveals escalating utilization in the vertical dimension and pronounced building space inequality. *Engineering* **47**, 86–99 (2025).
13. Esch, T. et al. World Settlement Footprint 3D—a first three-dimensional survey of the global building stock. *Remote Sens. Environ.* **270**, 112877 (2022).
14. Meijer, J. R., Huijbregts, M. A. J., Schotten, K. C. G. J. & Schipper, A. M. Global patterns of current and future road infrastructure. *Environ. Res. Lett.* **13**, 064006 (2018).
15. Huang, X., Yang, J., Wang, W. & Liu, Z. Mapping 10 m global impervious surface area (GISA-10m) using multi-source geospatial data. *Earth Syst. Sci. Data* **14**, 3649–3672 (2022).
16. Melchiorri, M., Pesaresi, M., Florczyk, A. J., Corbane, C. & Kemper, T. Principles and applications of the Global Human Settlement Layer as baseline for the land use efficiency indicator—SDG 11.3.1. *ISPRS Int. J. Geo-Inf.* **8**, 96 (2019).

17. Rousseau, L. S. A. et al. Material stock and embodied greenhouse gas emissions of global and urban road pavement. *Environ. Sci. Technol.* **56**, 18050–18059 (2022).
18. Haberl, H. et al. Weighing the global built environment: high-resolution mapping and quantification of material stocks in buildings. *J. Ind. Ecol.* **29**, 159–172 (2025).
19. Sun, J., Wang, T., Jiang, N., Liu, Z. & Gao, X. Gridded material stocks in China based on geographical and geometric configurations of the built-environment. *Sci. Data* **10**, 915 (2023).
20. Bettencourt, L. M. A. & Lobo, J. Urban scaling in Europe. *J. R. Soc. Interface* **13**, 20160005 (2016).
21. Kalt, G. et al. Material stocks in global electricity infrastructures—an empirical analysis of the power sector's stock-flow-service nexus. *Resour. Conserv. Recycl.* **173**, 105723 (2021).
22. Rosenthal, S. S. & Strange, W. C. Evidence on the nature and sources of agglomeration economies. In *Handbook of Regional and Urban Economics* Vol. 4 (eds Henderson, J. V. & Thisse, J.-F.) 2119–2171 (Elsevier, 2004).
23. Bettencourt, L. M. A., Lobo, J., Helbing, D., Kühnert, C. & West, G. B. Growth, innovation, scaling, and the pace of life in cities. *Proc. Natl Acad. Sci. USA* **104**, 7301–7306 (2007).
24. Park, R. E. & Burgess, E. W. *The City* (Univ. Chicago Press, 1925).
25. Gomez-Lievano, A., Youn, H. & Bettencourt, L. M. A. The statistics of urban scaling and their connection to Zipf's law. *PLoS ONE* **7**, e40393 (2012).
26. Wiedenhofer, D. et al. Mapping and modelling global mobility infrastructure stocks, material flows and their embodied greenhouse gas emissions. *J. Cleaner Prod.* **434**, 139742 (2024).
27. Dong, L., Huang, Z., Zhang, J. & Liu, Y. Understanding the mesoscopic scaling patterns within cities. *Sci. Rep.* **10**, 21201 (2020).
28. Schläpfer, M., Lee, J. & Bettencourt, L. M. A. Urban Skylines: building heights and shapes as measures of city size. Preprint at https://doi.org/10.48550/ARXIV.1512.00946 (2015).
29. Lehner, M. et al. Living smaller: acceptance, effects and structural factors in the EU. *Build. Cities* **5**, 215–230 https://doi.org/10.5334/bc.438 (2024).
30. González, M. C., Hidalgo, C. A. & Barabási, A.-L. Understanding individual human mobility patterns. *Nature* **453**, 779–782 (2008).
31. Louail, T. et al. From mobile phone data to the spatial structure of cities. *Sci. Rep.* **4**, 5276 (2014).
32. Alonso, W. *Location and Land Use: Toward a General Theory of Land Rent* (Harvard Univ. Press, 1964).
33. Liotta, C., Viguié, V. & Lepetit, Q. Testing the monocentric standard urban model in a global sample of cities. *Reg. Sci. Urban Econ.* **97**, 103832 (2022).
34. Gyourko, J. & Molloy, R. Regulation and housing supply. In *Handbook of Regional and Urban Economics* Vol. 5 (eds Duranton, G. et al.) 1289–1337 (Elsevier, 2015).
35. Cabeza, L. F. et al. Buildings. In *Climate Change 2022: Mitigation of Climate Change* (eds Shukla, P. R. et al.) (Cambridge Univ. Press, 2022).
36. United Nations Human Settlements Programme (UN-Habitat) *World Cities Report 2022: Envisaging the Future of Cities* https://doi.org/10.18356/9789210028592 (United Nations, 2022).
37. Güneralp, B. et al. Global scenarios of urban density and its impacts on building energy use through 2050. *Proc. Natl Acad. Sci. USA* **114**, 8945–8950 (2017).
38. Giuliano, G., Kang, S. & Yuan, Q. Agglomeration economies and evolving urban form. *Ann. Reg. Sci.* **63**, 377–398 (2019).
39. Koster, H. R. A. & Thisse, J.-F. Understanding spatial agglomeration: increasing returns, land, and transportation costs. *Annu. Rev. Econom.* **16**, 55–78 (2024).
40. Fischer, C. S. Toward a subcultural theory of urbanism. *Am. J. Sociol.* **80**, 1319–1341 (1975).
41. Rosenthal, S. S. & Strange, W. C. How close is close? The spatial reach of agglomeration economies. *J. Econ. Perspect.* **34**, 27–49 (2020).
42. Glaeser, E. L., Kallal, H. D., Scheinkman, J. A. & Shleifer, A. Growth in cities. *J. Polit. Econ.* **100**, 1126–1152 (1992).
43. Jacobs, J. *The Death and Life of Great American Cities* (Random House, 1961).
44. Storper, M. & Venables, A. J. Buzz: face-to-face contact and the urban economy. *J. Econ. Geogr.* **4**, 351–370 (2004).
45. McCulley, E. M. et al. Urban scaling of health outcomes: a scoping review. *J. Urban Health* **99**, 409–426 (2022).
46. Bettencourt, L. M. A., Lobo, J., Strumsky, D. & West, G. B. Urban scaling and its deviations: revealing the structure of wealth, innovation and crime across cities. *PLoS ONE* **5**, e13541 (2010).
47. Louf, R. & Barthelemy, M. How congestion shapes cities: from mobility patterns to scaling. *Sci. Rep.* **4**, 5561 (2014).
48. Tidwell, J. B. et al. Where shared sanitation is the only immediate option: a research agenda for shared sanitation in densely populated low-income urban settings. *Am. J. Trop. Med. Hyg.* **104**, 429–432 (2021).
49. Vélez-Henao, J. A. & Pauliuk, S. Material requirements of decent living standards. *Environ. Sci. Technol.* **57**, 14206–14217 (2023).
50. Batty, M. The size, scale, and shape of cities. *Science* **319**, 769–771 (2008).
51. Krausmann, F., Lauk, C., Haas, W. & Wiedenhofer, D. From resource extraction to outflows of wastes and emissions: the socioeconomic metabolism of the global economy, 1900–2015. *Glob. Environ. Change* **52**, 131–140 (2018).
52. Spawn, S. A., Sullivan, C. C., Lark, T. J. & Gibbs, H. K. Harmonized global maps of above and belowground biomass carbon density in the year 2010. *Sci. Data* **7**, 112 (2020).
53. Lu, M. & Hedin, L. O. Global plant–symbiont organization and emergence of biogeochemical cycles resolved by evolution-based trait modelling. *Nat. Ecol. Evol.* **3**, 239–250 (2019).
54. Bousquin, J. Discrete global grid systems as scalable geospatial frameworks for characterizing coastal environments. *Environ. Model. Softw.* **146**, 105210 (2021).
55. Goodall, B. *The Penguin Dictionary of Human Geography* (Penguin Books, 1987).
56. Mao, R., Bao, Y., Duan, H. & Liu, G. Global urban subway development, construction material stocks, and embodied carbon emissions. *Humanit. Soc. Sci. Commun.* **8**, 83 (2021).
57. van Engelenburg, M., Deetman, S., Fishman, T., Behrens, P. & van der Voet, E. TRIPI: a global dataset and codebase of the total resources in physical infrastructure encompassing road, rail, and parking. *Data Brief* **54**, 110387 (2024).
58. Thomson, D. R., Leasure, D. R., Bird, T., Tzavidis, N. & Tatem, A. J. How accurate are WorldPop-Global-Unconstrained gridded population data at the cell-level?: a simulation analysis in urban Namibia. *PLoS ONE* **17**, e0271504 (2022).
59. Bai, Z., Wang, J., Wang, M., Gao, M. & Sun, J. Accuracy assessment of multi-source gridded population distribution datasets in China. *Sustainability* **10**, 1363 (2018).
60. West, G. B. *Scale: The Universal Laws of Growth, Innovation, Sustainability, and the Pace of Life in Organisms, Cities, Economies, and Companies* (Penguin, 2017).
61. Galilei, G. *Dialogues Concerning Two New Sciences* (eds Crew, H. & de Salvio, A.) (Macmillan, 1914).
62. Niklas, K. J. & Hammond, S. T. On the interpretation of the normalization constant in the scaling equation. *Front. Ecol. Evol.* **6**, 212 (2019).
63. Glazier, D. S. Commentary: on the interpretation of the normalization constant in the scaling equation. *Front. Ecol. Evol.* **8**, 90 (2020).
64. Thomson, J. A. On growth and form. *Nature* **100**, 21–22 (1917).

65. Horder, T. J. D'arcy Wentworth Thompson, on growth and form (1917). In *Landmark Writings in Western Mathematics 1640–1940* (eds Grattan-Guinness et al.) 823–832 (Elsevier, 2005).
66. Kleiber, M. Body size and metabolism. *Hilgardia* **6**, 315–353 (1932).
67. Huxley, J. *Problems of Relative Growth* (Dover, 1972).
68. Bettencourt, L. M. A. *Introduction to Urban Science: Evidence and Theory of Cities as Complex Systems* https://doi.org/10.7551/mitpress/13909.001.0001 (MIT Press, 2021).
69. Kaitaniemi, P. How to derive biological information from the value of the normalization constant in allometric equations. *PLoS ONE* **3**, e1932 (2008).
70. Lumer, H. The relation between b and k in systems of relative growth functions of the form $y = bx^k$. *Am. Nat.* **70**, 188–191 (1936).
71. Fishman, T., Mastrucci, A., Peled, Y., Saxe, S. & van Ruijven, B. RASMI: global ranges of building material intensities differentiated by region, structure, and function. *Sci. Data* **11**, 418 (2024).
72. Clauset, A., Shalizi, C. R. & Newman, M. E. J. Power-law distributions in empirical data. *SIAM Rev.* **51**, 661–703 (2009).
73. Huang, K. & Lu, M. Nested economies of scale in global city mass. *figshare* https://doi.org/10.6084/m9.figshare.29482190 (2026).

Acknowledgements

We thank members of Lu lab (A. Zheng, J. Levine, I. Arroyo), K. Seto and members of Seto lab, J. Lobo and colleagues at the Department of Environmental Studies for helpful comments on the paper. We thank A. Zheng and L. Chen for creating illustrations.

Author contributions

K.H. and M.L. developed the overall conceptual framework, carried out analysis, designed visualization and wrote the paper together. Both authors contributed equally.

Funding

This work was supported by an internal grant from NYU Arts and Science (FRC 2024) to M.L. and K.H.

Competing interests

The authors declare no competing interests.

Additional information

Extended data is available for this paper at https://doi.org/10.1038/s44284-026-00532-x.

Supplementary information The online version contains supplementary material available at https://doi.org/10.1038/s44284-026-00532-x.

Correspondence and requests for materials should be addressed to Kangning Huang or Mingzhen Lu.

Peer review information *Nature Cities* thanks Luis Bettencourt, Dominik Wiedenhofer and the other, anonymous, reviewer(s) for their contribution to the peer review of this work. Peer reviewer reports are available.

Reprints and permissions information is available at www.nature.com/reprints.

Publisher's note Springer Nature remains neutral with regard to jurisdictional claims in published maps and institutional affiliations.

Open Access This article is licensed under a Creative Commons Attribution 4.0 International License, which permits use, sharing, adaptation, distribution and reproduction in any medium or format, as long as you give appropriate credit to the original author(s) and the source, provide a link to the Creative Commons licence, and indicate if changes were made. The images or other third party material in this article are included in the article's Creative Commons licence, unless indicated otherwise in a credit line to the material. If material is not included in the article's Creative Commons licence and your intended use is not permitted by statutory regulation or exceeds the permitted use, you will need to obtain permission directly from the copyright holder. To view a copy of this licence, visit http://creativecommons.org/licenses/by/4.0/.

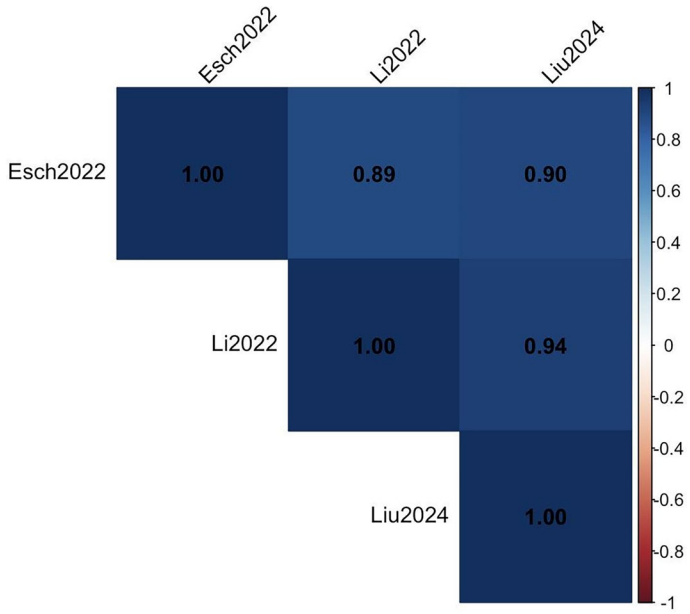
© The Author(s) 2026

https://doi.org/10.1038/s44284-026-00532-x



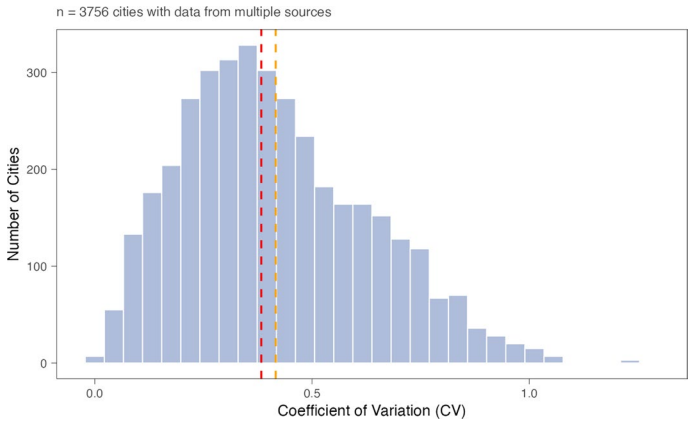
Extended Data Fig. 1 | Illustration of the city definition. Example cities across various continents demonstrate different scales of cities. Map data © OpenStreetMap (https://www.openstreetmap.org/copyright). Basemap tiles: Esri World Light Gray Canvas. Map image is the intellectual property of Esri and is used herein under license. Copyright © 2026 Esri and its licensors.

https://doi.org/10.1038/s44284-026-00532-x



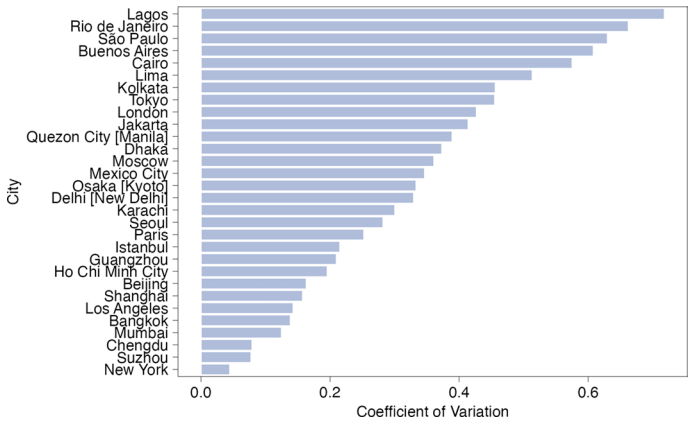
Extended Data Fig. 2 | Correlation matrix of building mass estimates across three global datasets. The heatmap shows Pearson correlation coefficients between city-level building mass estimates from Esch[13], Li[11], and Liu[12] datasets. Analysis includes cities with complete data across all three datasets (n = 3,721).

https://doi.org/10.1038/s44284-026-00532-x



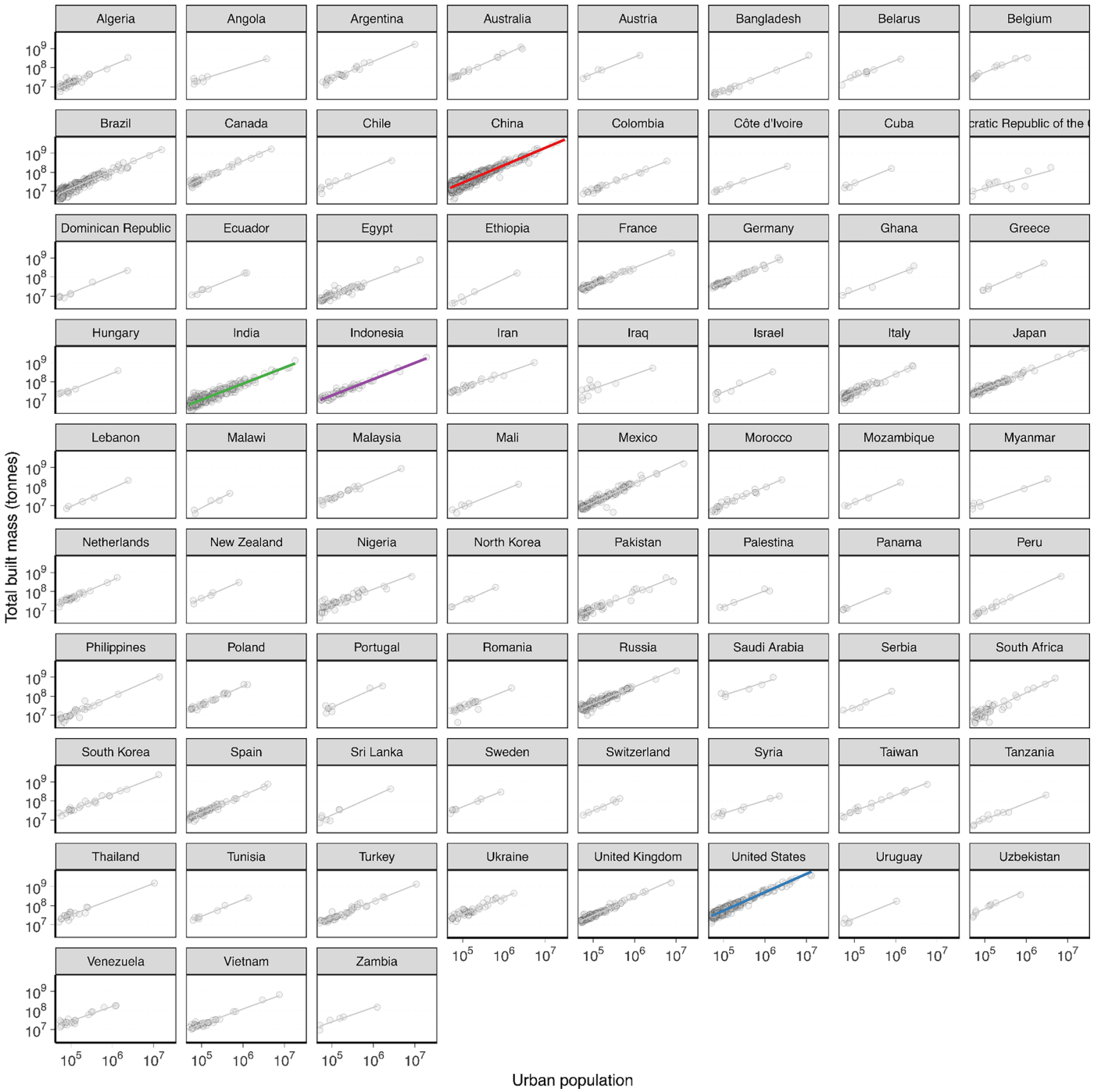
Extended Data Fig. 3 | Distribution of the coefficient of variation (CV) of urban building mass estimates across cities from multiple data sources. This histogram illustrates the distribution of the coefficient of variation (CV) of urban building mass estimates across cities, calculated from three global building volume datasets: Esch et al.[13], Li et al.[11], and Liu et al.[12]. The CV is derived as the ratio of standard deviation to mean building mass for each city, quantifying the relative variability between different data sources. Only cities with data available from at least two sources are included in the analysis (Zahedan, Iran is the only city with one source and is thus excluded from variability analysis). The red dashed line indicates the median CV, while the orange dashed line represents the mean CV.

https://doi.org/10.1038/s44284-026-00532-x



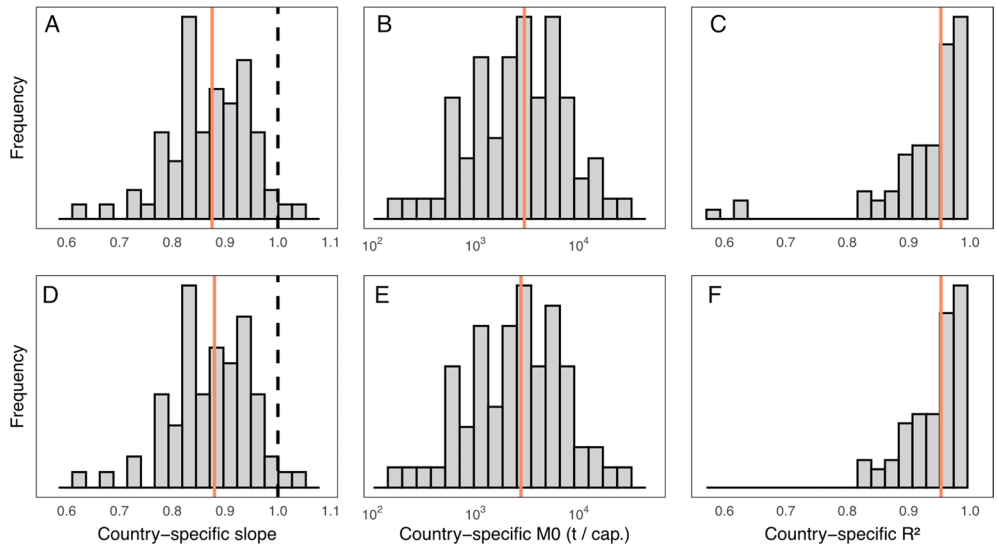
Extended Data Fig. 4 | Coefficient of variation in urban building mass estimates for the 30 most populous cities with multi-source data. Cities are ranked by CV magnitude, showing the relative variability in building mass estimates between the three global datasets (Esch et al.[13], Li et al.[11], and Liu et al.[12]). Higher values indicate greater disagreement between data sources for that particular city. Cities are selected based on 2015 population data and represent the largest urban areas where building mass estimates are available from multiple sources.

https://doi.org/10.1038/s44284-026-00532-x



Extended Data Fig. 5 | Sublinear urban scaling of built mass and its variation across all countries. We include the 74 countries meeting our criterion for inclusion (n_cities > 5).

https://doi.org/10.1038/s44284-026-00532-x



Extended Data Fig. 6 | Country-level scaling analysis statistics. The top row (**A**, **B**, **C**) includes all 74 countries with more than 5 cities, while the second row (**D**, **E**, **F**) excludes 3 countries with R^2 lower than 0.7. The overall country-level statistics are not sensitive to the inclusion of these 3 countries with relatively low goodness of fit.

nature portfolio

Corresponding author(s): Kangning Huang & Mingzhen Lu

Last updated by author(s): 08-28-2026

Reporting Summary

Nature Portfolio wishes to improve the reproducibility of the work that we publish. This form provides structure for consistency and transparency in reporting. For further information on Nature Portfolio policies, see our Editorial Policies and the Editorial Policy Checklist.

Statistics

For all statistical analyses, confirm that the following items are present in the figure legend, table legend, main text, or Methods section.

n/a	Confirmed	
☐	☒	The exact sample size (*n*) for each experimental group/condition, given as a discrete number and unit of measurement
☒	☐	A statement on whether measurements were taken from distinct samples or whether the same sample was measured repeatedly
☐	☒	The statistical test(s) used AND whether they are one- or two-sided *Only common tests should be described solely by name; describe more complex techniques in the Methods section.*
☒	☐	A description of all covariates tested
☒	☐	A description of any assumptions or corrections, such as tests of normality and adjustment for multiple comparisons
☐	☒	A full description of the statistical parameters including central tendency (e.g. means) or other basic estimates (e.g. regression coefficient) AND variation (e.g. standard deviation) or associated estimates of uncertainty (e.g. confidence intervals)
☒	☐	For null hypothesis testing, the test statistic (e.g. *F*, *t*, *r*) with confidence intervals, effect sizes, degrees of freedom and *P* value noted *Give P values as exact values whenever suitable.*
☒	☐	For Bayesian analysis, information on the choice of priors and Markov chain Monte Carlo settings
☒	☐	For hierarchical and complex designs, identification of the appropriate level for tests and full reporting of outcomes
☒	☐	Estimates of effect sizes (e.g. Cohen's *d*, Pearson's *r*), indicating how they were calculated

Our web collection on statistics for biologists contains articles on many of the points above.

Software and code

Policy information about availability of computer code

Data collection	We used publicly available datasets to collect data on global built structure, vegetation, and urban populations. Building volume data were obtained from Esch et al. (2022), Li et al. (2022), and Liu et al. (2024). Impervious surface data (roads and pavement) were from Huang et al. (2022). Vegetation biomass was from Spawn et al. (2020). Population data were extracted from the WorldPop project. Data processing and integration were conducted using R (v4.4.0) and its packages (zoo, lme4, stats). No custom code was required for data acquisition beyond dataset access and preprocessing.
Data analysis	All statistical analyses, scaling models, and simulations were conducted in R (v4.4.0). Universal scaling relationships were estimated by ordinary least squares on de-centered variables (stats::lm), following Bettencourt & Lobo (2016); mixed-effects models (lme4 v1.1-36) were used as a sensitivity comparison, and custom R scripts were used for simulations of scaling emergence. Figures were generated using R's base plotting functions and ggplot2. All code used for data analysis is publicly available together with the data on figshare at https://doi.org/10.6084/m9.figshare.29482190.

For manuscripts utilizing custom algorithms or software that are central to the research but not yet described in published literature, software must be made available to editors and reviewers. We strongly encourage code deposition in a community repository (e.g. GitHub). See the Nature Portfolio guidelines for submitting code & software for further information.

Data

Policy information about availability of data

All manuscripts must include a data availability statement. This statement should provide the following information, where applicable:

- Accession codes, unique identifiers, or web links for publicly available datasets
- A description of any restrictions on data availability
- For clinical datasets or third party data, please ensure that the statement adheres to our policy

All data supporting the findings of this study are publicly available on figshare at https://doi.org/10.6084/m9.figshare.29482190. An interactive visualization of these global mass patterns is available at https://city-mass.nested-complexity.net.

Research involving human participants, their data, or biological material

Policy information about studies with human participants or human data. See also policy information about sex, gender (identity/presentation), and sexual orientation and race, ethnicity and racism.

Reporting on sex and gender	NA
Reporting on race, ethnicity, or other socially relevant groupings	NA
Population characteristics	NA
Recruitment	NA
Ethics oversight	NA

Note that full information on the approval of the study protocol must also be provided in the manuscript.

Field-specific reporting

Please select the one below that is the best fit for your research. If you are not sure, read the appropriate sections before making your selection.

☐ Life sciences ☐ Behavioural & social sciences ☒ Ecological, evolutionary & environmental sciences

For a reference copy of the document with all sections, see nature.com/documents/nr-reporting-summary-flat.pdf

Life sciences study design

All studies must disclose on these points even when the disclosure is negative.

Sample size	*Describe how sample size was determined, detailing any statistical methods used to predetermine sample size OR if no sample-size calculation was performed, describe how sample sizes were chosen and provide a rationale for why these sample sizes are sufficient.*
Data exclusions	*Describe any data exclusions. If no data were excluded from the analyses, state so OR if data were excluded, describe the exclusions and the rationale behind them, indicating whether exclusion criteria were pre-established.*
Replication	*Describe the measures taken to verify the reproducibility of the experimental findings. If all attempts at replication were successful, confirm this OR if there are any findings that were not replicated or cannot be reproduced, note this and describe why.*
Randomization	*Describe how samples/organisms/participants were allocated into experimental groups. If allocation was not random, describe how covariates were controlled OR if this is not relevant to your study, explain why.*
Blinding	*Describe whether the investigators were blinded to group allocation during data collection and/or analysis. If blinding was not possible, describe why OR explain why blinding was not relevant to your study.*

Behavioural & social sciences study design

All studies must disclose on these points even when the disclosure is negative.

Study description	*Briefly describe the study type including whether data are quantitative, qualitative, or mixed-methods (e.g. qualitative cross-sectional, quantitative experimental, mixed-methods case study).*
Research sample	*State the research sample (e.g. Harvard university undergraduates, villagers in rural India) and provide relevant demographic*

Research sample	*information (e.g. age, sex) and indicate whether the sample is representative. Provide a rationale for the study sample chosen. For studies involving existing datasets, please describe the dataset and source.*
Sampling strategy	*Describe the sampling procedure (e.g. random, snowball, stratified, convenience). Describe the statistical methods that were used to predetermine sample size OR if no sample-size calculation was performed, describe how sample sizes were chosen and provide a rationale for why these sample sizes are sufficient. For qualitative data, please indicate whether data saturation was considered, and what criteria were used to decide that no further sampling was needed.*
Data collection	*Provide details about the data collection procedure, including the instruments or devices used to record the data (e.g. pen and paper, computer, eye tracker, video or audio equipment) whether anyone was present besides the participant(s) and the researcher, and whether the researcher was blind to experimental condition and/or the study hypothesis during data collection.*
Timing	*Indicate the start and stop dates of data collection. If there is a gap between collection periods, state the dates for each sample cohort.*
Data exclusions	*If no data were excluded from the analyses, state so OR if data were excluded, provide the exact number of exclusions and the rationale behind them, indicating whether exclusion criteria were pre-established.*
Non-participation	*State how many participants dropped out/declined participation and the reason(s) given OR provide response rate OR state that no participants dropped out/declined participation.*
Randomization	*If participants were not allocated into experimental groups, state so OR describe how participants were allocated to groups, and if allocation was not random, describe how covariates were controlled.*

Ecological, evolutionary & environmental sciences study design

All studies must disclose on these points even when the disclosure is negative.

Study description	This study quantifies global patterns of urban built mass and its scaling with population size at both city and neighborhood levels. We integrated multiple high-resolution spatial datasets (buildings, roads, pavements, population, vegetation biomass) to construct a global database of >3,000 cities. Statistical analyses and theoretical models were used to test for economies of scale across nested urban structures.
Research sample	The research sample consisted of cities worldwide with populations greater than 50,000, as defined by the Global Human Settlement Layer (GHSL). Within cities, neighborhoods were defined using the H3 global hexagonal grid (~36 km² per cell). This design captures both across-city and within-city variation, allowing for multiscale analysis of built mass and population relationships.
Sampling strategy	All cities meeting the population threshold (≥50,000 residents, a commonly used city cutoff) were included, ensuring global coverage rather than a subsample. For neighborhood-level analyses, all grid cells intersecting city boundaries were used. No additional sampling was performed. This exhaustive inclusion guarantees representativeness across regions, economic contexts, and urban forms.
Data collection	We used publicly available datasets: global building volumes (Esch et al. 2022; Li et al. 2022; Liu et al. 2024), impervious surfaces and pavements (Huang et al. 2022), global vegetation biomass (Spawn et al. 2020), and population (WorldPop). Data were processed and harmonized using R scripts, with material intensities applied from Haberl et al. (2025). No new field data were collected.
Timing and spatial scale	Data reflect global conditions around the 2010–2020 period, depending on the source dataset (e.g., vegetation biomass for 2010, WorldPop annual estimates, global built environment datasets published 2022–2024). The spatial scale includes cities globally (>3,000 cities across 75 countries) and their subdivisions into hexagonal neighborhoods (~3.7 km radius).
Data exclusions	No data were excluded, except for cities with incomplete or inconsistent coverage across datasets (e.g., missing building volume estimates). Pre-established criteria required at least two independent building volume datasets for inclusion in cross-validation of city-scale estimates.
Reproducibility	All data sources are publicly available, and analysis was performed using reproducible R scripts. Key results (scaling exponents, regression outputs, simulations) can be replicated by re-running the code with the provided datasets. Code and data are publicly deposited on figshare at https://doi.org/10.6084/m9.figshare.29482190.
Randomization	NA. The study relies on global observational datasets, not experimental manipulations. Cities and neighborhoods were analyzed exhaustively rather than randomly sampled.
Blinding	NA. Data analysis involved quantitative, spatially explicit datasets with no subjective scoring or observer bias.

Did the study involve field work? ☐ Yes ☒ No

Field work, collection and transport

Field conditions	NA

Location	NA
Access & import/export	NA
Disturbance	NA

Reporting for specific materials, systems and methods

We require information from authors about some types of materials, experimental systems and methods used in many studies. Here, indicate whether each material, system or method listed is relevant to your study. If you are not sure if a list item applies to your research, read the appropriate section before selecting a response.

Materials & experimental systems

n/a	Involved in the study
☒	☐ Antibodies
☒	☐ Eukaryotic cell lines
☒	☐ Palaeontology and archaeology
☒	☐ Animals and other organisms
☒	☐ Clinical data
☒	☐ Dual use research of concern
☒	☐ Plants

Methods

n/a	Involved in the study
☒	☐ ChIP-seq
☒	☐ Flow cytometry
☒	☐ MRI-based neuroimaging

Antibodies

Antibodies used	*Describe all antibodies used in the study; as applicable, provide supplier name, catalog number, clone name, and lot number.*
Validation	*Describe the validation of each primary antibody for the species and application, noting any validation statements on the manufacturer's website, relevant citations, antibody profiles in online databases, or data provided in the manuscript.*

Eukaryotic cell lines

Policy information about cell lines and Sex and Gender in Research

Cell line source(s)	*State the source of each cell line used and the sex of all primary cell lines and cells derived from human participants or vertebrate models.*
Authentication	*Describe the authentication procedures for each cell line used OR declare that none of the cell lines used were authenticated.*
Mycoplasma contamination	*Confirm that all cell lines tested negative for mycoplasma contamination OR describe the results of the testing for mycoplasma contamination OR declare that the cell lines were not tested for mycoplasma contamination.*
Commonly misidentified lines (See ICLAC register)	*Name any commonly misidentified cell lines used in the study and provide a rationale for their use.*

Palaeontology and Archaeology

Specimen provenance	*Provide provenance information for specimens and describe permits that were obtained for the work (including the name of the issuing authority, the date of issue, and any identifying information). Permits should encompass collection and, where applicable, export.*
Specimen deposition	*Indicate where the specimens have been deposited to permit free access by other researchers.*
Dating methods	*If new dates are provided, describe how they were obtained (e.g. collection, storage, sample pretreatment and measurement), where they were obtained (i.e. lab name), the calibration program and the protocol for quality assurance OR state that no new dates are provided.*

☐ Tick this box to confirm that the raw and calibrated dates are available in the paper or in Supplementary Information.

Ethics oversight	*Identify the organization(s) that approved or provided guidance on the study protocol, OR state that no ethical approval or guidance was required and explain why not.*

Note that full information on the approval of the study protocol must also be provided in the manuscript.

Animals and other research organisms

Policy information about studies involving animals; ARRIVE guidelines recommended for reporting animal research, and Sex and Gender in Research

Laboratory animals	*For laboratory animals, report species, strain and age OR state that the study did not involve laboratory animals.*
Wild animals	*Provide details on animals observed in or captured in the field; report species and age where possible. Describe how animals were caught and transported and what happened to captive animals after the study (if killed, explain why and describe method; if released, say where and when) OR state that the study did not involve wild animals.*
Reporting on sex	*Indicate if findings apply to only one sex; describe whether sex was considered in study design, methods used for assigning sex. Provide data disaggregated for sex where this information has been collected in the source data as appropriate; provide overall numbers in this Reporting Summary. Please state if this information has not been collected. Report sex-based analyses where performed, justify reasons for lack of sex-based analysis.*
Field-collected samples	*For laboratory work with field-collected samples, describe all relevant parameters such as housing, maintenance, temperature, photoperiod and end-of-experiment protocol OR state that the study did not involve samples collected from the field.*
Ethics oversight	*Identify the organization(s) that approved or provided guidance on the study protocol, OR state that no ethical approval or guidance was required and explain why not.*

Note that full information on the approval of the study protocol must also be provided in the manuscript.

Clinical data

Policy information about clinical studies

All manuscripts should comply with the ICMJE guidelines for publication of clinical research and a completed CONSORT checklist must be included with all submissions.

Clinical trial registration	*Provide the trial registration number from ClinicalTrials.gov or an equivalent agency.*
Study protocol	*Note where the full trial protocol can be accessed OR if not available, explain why.*
Data collection	*Describe the settings and locales of data collection, noting the time periods of recruitment and data collection.*
Outcomes	*Describe how you pre-defined primary and secondary outcome measures and how you assessed these measures.*

Dual use research of concern

Policy information about dual use research of concern

Hazards

Could the accidental, deliberate or reckless misuse of agents or technologies generated in the work, or the application of information presented in the manuscript, pose a threat to:

No	Yes	
☐	☐	Public health
☐	☐	National security
☐	☐	Crops and/or livestock
☐	☐	Ecosystems
☐	☐	Any other significant area

Experiments of concern

Does the work involve any of these experiments of concern:

No	Yes	
☐	☐	Demonstrate how to render a vaccine ineffective
☐	☐	Confer resistance to therapeutically useful antibiotics or antiviral agents
☐	☐	Enhance the virulence of a pathogen or render a nonpathogen virulent
☐	☐	Increase transmissibility of a pathogen
☐	☐	Alter the host range of a pathogen
☐	☐	Enable evasion of diagnostic/detection modalities
☐	☐	Enable the weaponization of a biological agent or toxin
☐	☐	Any other potentially harmful combination of experiments and agents

Plants

Seed stocks: NA

Novel plant genotypes: NA

Authentication: NA

ChIP-seq

Data deposition

☐ Confirm that both raw and final processed data have been deposited in a public database such as GEO.

☐ Confirm that you have deposited or provided access to graph files (e.g. BED files) for the called peaks.

Data access links
May remain private before publication.

For "Initial submission" or "Revised version" documents, provide reviewer access links. For your "Final submission" document, provide a link to the deposited data.

Files in database submission

Provide a list of all files available in the database submission.

Genome browser session
(e.g. UCSC)

Provide a link to an anonymized genome browser session for "Initial submission" and "Revised version" documents only, to enable peer review. Write "no longer applicable" for "Final submission" documents.

Methodology

Replicates

Describe the experimental replicates, specifying number, type and replicate agreement.

Sequencing depth

Describe the sequencing depth for each experiment, providing the total number of reads, uniquely mapped reads, length of reads and whether they were paired- or single-end.

Antibodies

Describe the antibodies used for the ChIP-seq experiments; as applicable, provide supplier name, catalog number, clone name, and lot number.

Peak calling parameters

Specify the command line program and parameters used for read mapping and peak calling, including the ChIP, control and index files used.

Data quality

Describe the methods used to ensure data quality in full detail, including how many peaks are at FDR 5% and above 5-fold enrichment.

Software

Describe the software used to collect and analyze the ChIP-seq data. For custom code that has been deposited into a community repository, provide accession details.

Flow Cytometry

Plots

Confirm that:

☐ The axis labels state the marker and fluorochrome used (e.g. CD4-FITC).

☐ The axis scales are clearly visible. Include numbers along axes only for bottom left plot of group (a 'group' is an analysis of identical markers).

☐ All plots are contour plots with outliers or pseudocolor plots.

☐ A numerical value for number of cells or percentage (with statistics) is provided.

Methodology

Sample preparation	*Describe the sample preparation, detailing the biological source of the cells and any tissue processing steps used.*
Instrument	*Identify the instrument used for data collection, specifying make and model number.*
Software	*Describe the software used to collect and analyze the flow cytometry data. For custom code that has been deposited into a community repository, provide accession details.*
Cell population abundance	*Describe the abundance of the relevant cell populations within post-sort fractions, providing details on the purity of the samples and how it was determined.*
Gating strategy	*Describe the gating strategy used for all relevant experiments, specifying the preliminary FSC/SSC gates of the starting cell population, indicating where boundaries between "positive" and "negative" staining cell populations are defined.*

☐ Tick this box to confirm that a figure exemplifying the gating strategy is provided in the Supplementary Information.

Magnetic resonance imaging

Experimental design

Design type	*Indicate task or resting state; event-related or block design.*
Design specifications	*Specify the number of blocks, trials or experimental units per session and/or subject, and specify the length of each trial or block (if trials are blocked) and interval between trials.*
Behavioral performance measures	*State number and/or type of variables recorded (e.g. correct button press, response time) and what statistics were used to establish that the subjects were performing the task as expected (e.g. mean, range, and/or standard deviation across subjects).*

Acquisition

Imaging type(s)	*Specify: functional, structural, diffusion, perfusion.*
Field strength	*Specify in Tesla*
Sequence & imaging parameters	*Specify the pulse sequence type (gradient echo, spin echo, etc.), imaging type (EPI, spiral, etc.), field of view, matrix size, slice thickness, orientation and TE/TR/flip angle.*
Area of acquisition	*State whether a whole brain scan was used OR define the area of acquisition, describing how the region was determined.*

Diffusion MRI ☐ Used ☐ Not used

Preprocessing

Preprocessing software	*Provide detail on software version and revision number and on specific parameters (model/functions, brain extraction, segmentation, smoothing kernel size, etc.).*
Normalization	*If data were normalized/standardized, describe the approach(es): specify linear or non-linear and define image types used for transformation OR indicate that data were not normalized and explain rationale for lack of normalization.*
Normalization template	*Describe the template used for normalization/transformation, specifying subject space or group standardized space (e.g. original Talairach, MNI305, ICBM152) OR indicate that the data were not normalized.*
Noise and artifact removal	*Describe your procedure(s) for artifact and structured noise removal, specifying motion parameters, tissue signals and physiological signals (heart rate, respiration).*

Volume censoring

Define your software and/or method and criteria for volume censoring, and state the extent of such censoring.

Statistical modeling & inference

Model type and settings

Specify type (mass univariate, multivariate, RSA, predictive, etc.) and describe essential details of the model at the first and second levels (e.g. fixed, random or mixed effects; drift or auto-correlation).

Effect(s) tested

Define precise effect in terms of the task or stimulus conditions instead of psychological concepts and indicate whether ANOVA or factorial designs were used.

Specify type of analysis: ☐ Whole brain ☐ ROI-based ☐ Both

Statistic type for inference

Specify voxel-wise or cluster-wise and report all relevant parameters for cluster-wise methods.

(See Eklund et al. 2016)

Correction

Describe the type of correction and how it is obtained for multiple comparisons (e.g. FWE, FDR, permutation or Monte Carlo).

Models & analysis

n/a	Involved in the study
☐	☐ Functional and/or effective connectivity
☐	☐ Graph analysis
☐	☐ Multivariate modeling or predictive analysis

Functional and/or effective connectivity

Report the measures of dependence used and the model details (e.g. Pearson correlation, partial correlation, mutual information).

Graph analysis

Report the dependent variable and connectivity measure, specifying weighted graph or binarized graph, subject- or group-level, and the global and/or node summaries used (e.g. clustering coefficient, efficiency, etc.).

Multivariate modeling and predictive analysis

Specify independent variables, features extraction and dimension reduction, model, training and evaluation metrics.